DOI: 10.1002/ejic.200901133

Building Niobate Nanoparticles with Hexaniobate Lindqvist Ions

Hua Tong[a] and Jinhua Ye*[a]

Keywords: Niobium / Nanoparticles / Lindqvist ions / Synthetic methods

We present a general method to fabricate niobate nanoparticles (NPs) by using hexaniobate Lindqvist ions as niobium source. First, soft-chemical synthesis was adopted to prepare amorphous compound NPs, which subsequently served as parent bodies, affording not only nanoscale size but also optimal compositions and elements for the final annealed nanocrystalline niobates. By this method, a series of nanocrystalline niobates, including $MNbO_4$ (M = In, Ga, Fe), MNb_2O_6 (M = Ba, Sr, Ni, Cd, Pb), $M_xFe_{1-x}NbO_4$ (M = In, Ga), $M_xNi_{1-x}Nb_2O_6$ (M = Ba, Sr), and $(AgNb)_{1-x}(SrTi)_xO_3$, were successfully prepared. Experimental results presented herein show that the compositions and components of niobate NPs can be adjusted as desired, markedly influencing the crystal phase, energy band structure, and photocatalytic performance of the niobate NPs.

1. Introduction

The entire world is confronted by severe energy and environmental issues attributable to immoderate consumption of fossil fuels and poisonous chemicals. Over the past 30 years, photocatalysis has been developing rapidly for production of clean hydrogen fuel from water and elimination of poisonous chemicals. In 1972, Fujishima et al. reported the famous Honda–Fujishima effect and obtained hydrogen by splitting water molecules by using titanium oxide as a photocatalyst.[1] Since then, numerous and various inorganic materials have been studied. A comprehensive survey of photocatalytic activity, chemical stability, and environmental friendliness shows that the most promising photocatalysts might be titanium, niobium, or tantalum-based materials. For example, nickel-doped indium tantalate (Ni-$InTaO_4$) was first reported to split water overall under visible light;[2] lanthanum-doped sodium tantalate (La-Na-TaO_3) holds the record of highest efficiency in splitting water under UV light;[3] and $(AgNb)_{1-x}(SrTi)_xO_3$[4,5] and N-HNb_3O_8[6] represent the materials responsible for the visible-light-induced degradation of gaseous organic molecules and liquid dyes, respectively. Materials for photocatalytic hydrogen production have been well reviewed recently by Osterloh[7] and Navarro et al.[8]

To improve their performance further, preparing nanosized photocatalysts presents an efficient strategy, because of their adjustable band gap, stronger photon absorption, larger specific surface area, and a shorter pathway for carrier transfer. In cases of niobate nanomaterials for photocatalytic applications, $LiNbO_3$,[9] $KNbO_3$,[10] KNb_3O_8,[11] $K_4Nb_6O_{17}$,[12–14] $SrNb_2O_6$,[15] $Sr_2Nb_2O_7$,[15] $Ca_2Nb_3O_{10}$,[16–18] $InNbO_4$,[19] etc., shaped as nanoparticles (NPs), nanorods, nanowires, and nanosheets, were synthesized; they showed improved photocatalytic activity relative to their respective bulk materials. However, because of the scarcity of powerful synthetic methods, it is noteworthy that almost all significant progress achieved in niobate nanomaterials to date has mainly centered upon the s-block alkali and alkaline-earth metal niobates,[9–18,20–28] and more rarely on the d-block and p-block metal niobates. Although Nb_2O_5, which can be used with hydrothermal methods, was widely adopted and led to most of the alkali metal niobate nanomaterials,[9–11,13,15,20–24,26,27] the method seems barely applicable for other kinds of niobates, because only alkali metal ions can meet the demands of good stability in a strongly basic aqueous solution. Under basic hydrothermal conditions, Nb_2O_5 can be transformed into polyoxoniobate anions such as $[Nb_6O_{19}]^{8-}$,[29,30] $[Nb_{10}O_{28}]^{6-}$,[31,32] etc., which might be combined with some metal cations to construct niobate nanomaterials. A few niobate nanomaterials have been synthesized by using other special methods, such as sol–gel,[28] molten salt,[33] and solvent-thermal[34] processing. However, these methods are not widely applicable, because of their inherent chemical and technical limitations. Recently, complex multicomponent niobates, especially solid solutions such as $(AgNb)_{1-x}(SrTi)_xO_3$[4,5] and $Ag_xNa_{1-x}NbO_3$,[35] etc., have received much more attention, because these materials provide a mode of adjusting energy band structures upon compositions to optimize their photocatalytic efficiency. The synthesis of niobate nanomaterials of this kind is not only of intense interest, it is also a great challenge. Consequently, a general synthetic route by which niobate

[a] International Center for Materials Nanoarchitectonics (MANA), and Photocatalytic Materials Center
National Institute for Materials Science (NIMS)
1-2-1 Sengen, Tsukuba, Ibaraki 305-0047, Japan
Fax: +81-29-859-2301
E-mail: Jinhua.YE@nims.go.jp

Supporting information for this article is available on the WWW under http://dx.doi.org/10.1002/ejic.200901133.

nanomaterials can be built from atoms or molecules in a homogeneous system is highly anticipated. In this way, niobate nanomaterials with adjustable composition and uniform size and morphology can be easily achieved. To fulfil this idea, an appropriate niobium precursor with good solubility in a certain solvent is required. However, this requirement cannot be satisfied by the typically used Nb_2O_5 or $NbCl_5$, each of which has poor solubility or stability towards hydrolysis in aqueous solution.

To date, no evidence has been presented for the existence of isolated niobium atoms or ions in aqueous solution. However, hexaniobate Lindqvist ion $[Nb_6O_{19}]^{8-}$, the most dominant and smallest of its kind,[30] has been well studied and used as the standard architecture for heteropolyniobates.[30,36–40] Very recently, Nyman et al. reported the rare earth niobates and tantalates prepared by hydrothermal synthesis by utilizing the Lindqvist ions $[Nb_6O_{19}]^{8-}$ and $[Ta_6O_{19}]^{8-}$.[41,42] In this article, we present a general method to build niobate NPs by using hexaniobate ions as a niobium source. Two types of niobate NPs are reported here. One is yttrium-based niobate NPs that can split water to release hydrogen, and the other is silver-based niobate NPs that can degrade gaseous organic molecules.

2. Results and Discussion

2.1 Hexaniobate Lindqvist Ions

In previous reports in the literature,[30,36–40] a simple method was reported to prepare hexaniobate ions in aqueous solution. Briefly, it was to dissolve amorphous $Nb_2O_5{\cdot}xH_2O$ in a strongly basic aqueous solution of inorganic alkali hydroxides (e.g. NaOH or KOH). In our experiment, organic ethanolamine instead of inorganic alkali hydroxides was used as basic reagent, which led to a non-alkali-metal hexaniobate solution. Consequently, alkali metal impurities could be excluded from the final niobate products. The presence of hexaniobate ions in aqueous solution could be evidenced by analyzing the precipitates that separate out of the solution when excess ethanol was added. The precipitates out of a sodium hexaniobate aqueous solution, in which sodium hydroxide or ethanolamine was used as the basic reagent, were $Na_7(HNb_6O_{19}){\cdot}15H_2O$ crystallites (see Figure S1 in the Supporting Information). Although the precipitates (P1) of our non-alkali-metal hexaniobate solution were amorphous compounds, they had molecular vibrational characteristics identical with those of $Na_7(HNb_6O_{19}){\cdot}15H_2O$ crystallites, as shown in the Raman and IR spectra in Figure 1. It was possible to assign all Raman and IR bands presented in Figure 1(a) and (b) to the vibrational modes of hexaniobate ions according to available studies.[38,43] Figure 1(a) also shows that the Raman bands of P1 are wider than those of $Na_7(HNb_6O_{19}){\cdot}15H_2O$ crystallites, which is expected to be the consequence of disordered accumulation of hexaniobate ions in P1. In contrast, hexaniobate ions were arranged periodically in $Na_7(HNb_6O_{19}){\cdot}15H_2O$ crystallites. Both P1 and $Na_7(HNb_6O_{19}){\cdot}15H_2O$ crystallites can be dissolved reversibly in pure water. The points presented above indicate the presence of hexaniobate ions in the aqueous solution that we prepared.

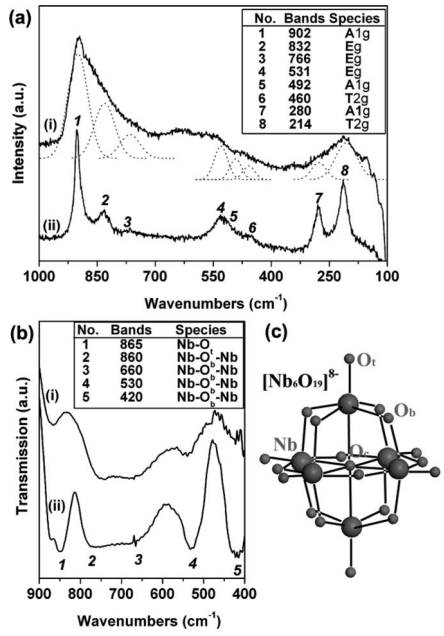

Figure 1. (a) Raman spectra and (b) IR spectra of (i) amorphous non-alkali-metal hexaniobate compounds (P1) and (ii) $Na_7(HNb_6O_{19}){\cdot}15H_2O$ crystallites. (c) A ball-and-stick representation of a $(Nb_6O_{19})^{8-}$ cluster: O_c (central oxygen), O_t (terminal oxygen), and O_b (bridging oxygen).

2.2 Formation of Niobate NPs

The non-alkali-metal hexaniobate aqueous solution was basic (pH = ca. 10.8), which results from the presence of 2% (v/v) ethanolamine. However, an acidic niobium precursor solution is expected to favor the simultaneous dissolution of other metal ions, which might be beneficial for the homogeneous growth of NPs in solution. Usually, in acidic aqueous solution (pH < 7), the hexaniobate ions are not stable; they hydrolyze and precipitate as hydrous niobium oxide $Nb_2O_5{\cdot}xH_2O$. Fortunately, we found that hexaniobate ions are stable in the aqueous solution of citric acid. Even if the pH value were adjusted to approximately 2, the solution remained clear and colorless. A possible reason is that the hexaniobate ions combined with citric acid molecules to form new complex compounds that are water soluble.

The fabrication of nanocrystalline niobates involved two steps: soft-chemical synthesis and annealing crystallization. In the first step, the precursor hexaniobate solution, with addition of citric acid (pH was adjusted to ca. 4.8) and stoichiometric amounts of metal salts went though a microwave-assisted hydrothermal process to afford amorphous compound NPs. These amorphous compound NPs served

as parent bodies in the next step, affording not only the nanoscale size but also the required compositions and elements for the final annealed nanocrystalline niobates. The highest temperature (250 °C) that our hydrothermal system can provide is less than the temperature for crystallization of niobate NPs, except for nanocrystalline $InNbO_4$ (Figure S2). Therefore, an annealing step was necessary for obtaining nanocrystalline niobates. Reportedly, nanocrystalline alkali and alkaline-earth-metal niobates can be synthesized hydrothermally in strongly basic systems but not in acidic systems. Although our synthetic method seems somewhat inconvenient, it was easy to fabricate complex multicomponent nanocrystalline niobates. Moreover, some metal ions that are prone to reduction under hydrothermal conditions might be easily impregnated with amorphous compound NPs by the ion-exchange method, such as in the case of silver-based niobate NPs, which will be discussed in a later section.

The amorphous compound NPs were formed by the reaction of negatively charged hexaniobate and positively charged metal ions. The polymerization of hexaniobate ions in the hydrothermal process defined the morphology, size, and amorphous atomic framework of amorphous compound NPs. This conclusion could be drawn on the basis of the following evidence: (1) when no other metal ion was involved, hexaniobate ions polymerized into amorphous hydrous niobium oxide $Nb_2O_5{\cdot}xH_2O$ NPs with a size of about 10 nm [Figure S3(a)]; (2) if neither other metal ions nor citric acid was present, the polymers of hexaniobate ions would be curly amorphous hydrous niobium oxide $Nb_2O_5{\cdot}xH_2O$ nanosheets [Figure S3(b)]; and (3) in another hydrothermal synthesis free of hexaniobate ions, non-uniform metal oxides or hydroxides were generated in aqueous solution containing citric acid and ethanolamine. The precursor solution remained clear, and no solid product was generated until the temperature was greater than 170 °C, at which the polymerization of hexaniobate ions was triggered. Results show that the finished hydrothermal solution gave off CO_2 gas and that its pH value changed from the acidic to the basic range (pH > 9), because of the decomposition of citric acid (ca. 175 °C under air pressure) and the hence increased proportion of ethanolamine relative to citric acid. Therefore, it is assumed that the metal ions (but the alkali metal ions), which are unstable towards hydrolysis in basic aqueous solution, might be fully combined with hexaniobate ions into amorphous compound NPs. The metallic composition of an amorphous compound NP can be controlled depending on which and how many metal ions are supplied. For example, in a hexaniobate solution, addition of yttrium nitrate (at a 1:1 Nb/Y molar ratio) led to the preparation of yttrium/niobium-based amorphous compound NPs through a hydrothermal reaction [inset in Figure 2(a)]. Figure 2(a) presents a typical energy-dispersive X-ray spectroscopy (EDS) spectrum of the bulk of these NPs. According to the EDS calculation, these NPs contain the elements niobium and yttrium in an almost 1:1 molar ratio. The same result was also obtained for a single NP [Figure 2(b)], further verifying our supposition.

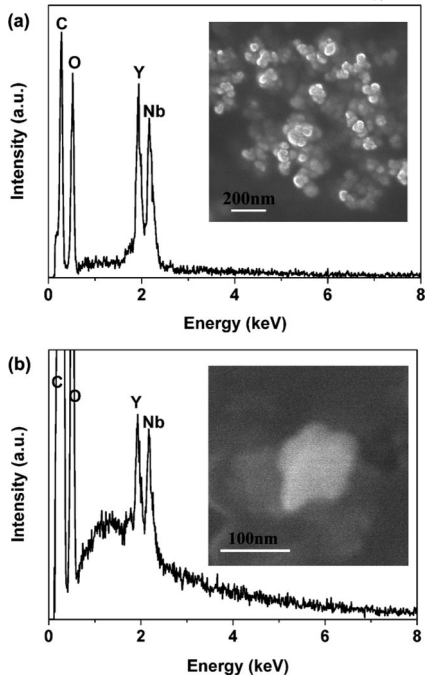

Figure 2. Yttrium/niobium-based amorphous compound NPs (before annealing): (a) EDS spectrum of the bulk of NPs and (b) EDS spectrum of a single NP. Insets are SEM images.

The final crystallized niobate NPs were formed through fast calcination at high temperature in a short time to suppress the growth of niobate NPs. On the basis of TG-DTA analysis (Figure S4), the optimum calcination temperature for crystallization of niobate NPs was determined. Figure 3 shows the nanocrystalline yttrium-based niobates that were taken as examples. The SEM images [Figure 3(a1)–(d1)] and TEM images [Figure 3(a2)–(d2)] reveal that these yttrium-based niobate NPs have sizes in the range 20–40 nm. The HRTEM images [Figure 3(a3)–(d3)] indicate that these niobate NPs are isolated and well crystallized. By comparing the SEM image before annealing [inset in Figure 2(a)] with that after annealing [Figure 3(a1)], it can be concluded that the $YNbO_4$ NPs inherited their morphology and size from the parent NPs.

2.3 Phase and Composition of Niobate NPs

The as-prepared ternary niobate NPs $MNbO_4$ (M = Y, La, In, Ga, Fe) and MNb_2O_6 (M = Ba, Sr, Ni, Cd, Pb) were of pure single-crystal phase, which can be obtained by simply controlling the stoichiometry of additions to the initial solutions. However, the situation is more complicated for the crystal phase of the multicomponent niobate NPs. For the quaternary yttrium-based niobates, the $Y_{1-x}La_xNbO_4$ NPs are considered as a solid solution of $YNbO_4$ and $LaNbO_4$. The respectively prepared $YNbO_4$ and $LaNbO_4$ NPs had the same tetragonal crystallographic structure and close lattice constants. Figure 3(e) shows that the $Y_{0.5}La_{0.5}NbO_4$ NPs have a crystallographic structure

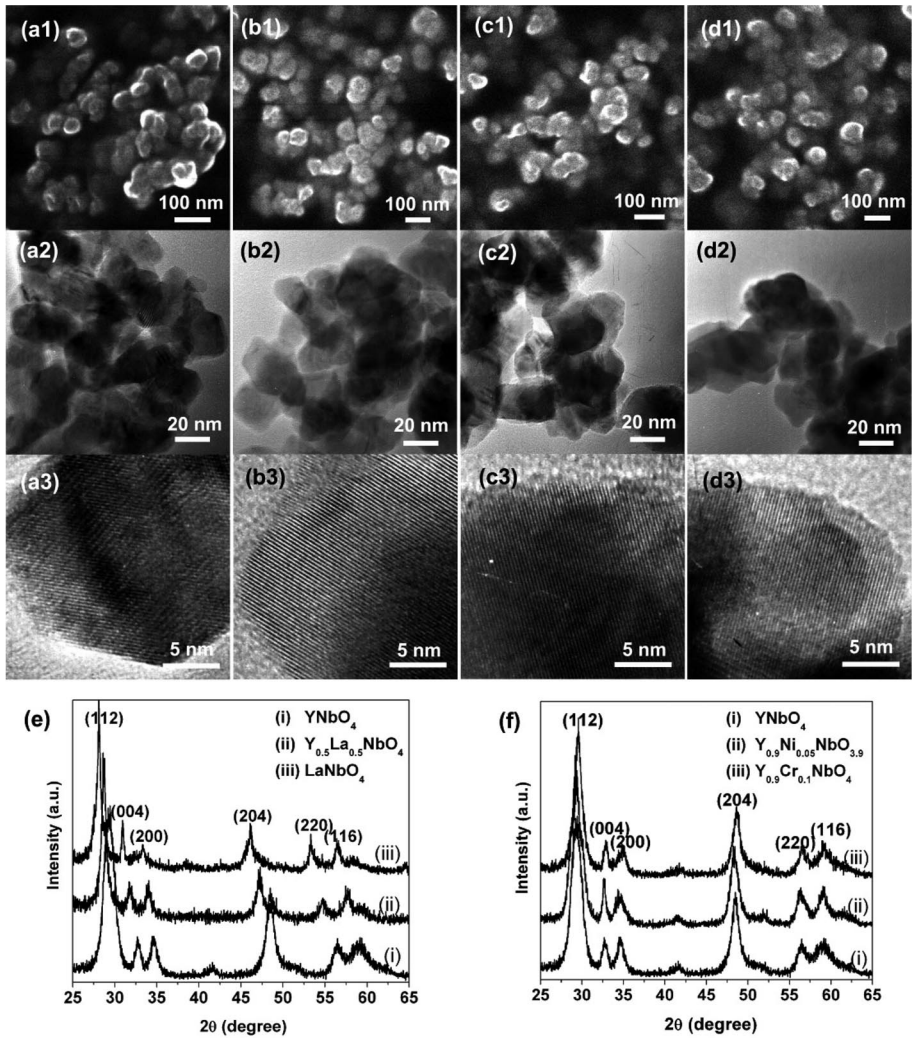

Figure 3. Nanocrystalline yttrium-based niobates (after annealing): (a1–d1) SEM images, (a2–d2) TEM images, and (a3–d3) HRTEM images of (a) $YNbO_4$, (b) $Y_{0.5}La_{0.5}NbO_4$, (c) $Y_{0.9}Cr_{0.1}NbO_4$, (d) $Y_{0.9}Ni_{0.05}NbO_{3.9}$; (e, f) XRD patterns.

coincident with those of $YNbO_4$ and $LaNbO_4$ NPs and its lattice constants lie between those of the $YNbO_4$ and $LaNbO_4$ NPs. This implies that the single phase of $Y_xLa_{1-x}NbO_4$ NPs might be composed of any ratio of yttrium and lanthanum atoms. Furthermore, the $M_xFe_{1-x}NbO_4$ (M = In, Ga) NPs are also one kind of solid solution (Figure S5). For $Y_{1-x}Cr_xNbO_4$ or $Y_{1-2x}Ni_xNbO_{4-2x}$ NPs, small amounts of chromium or nickel are confined in the pure tetragonal phases of the NPs, such as in the samples of $Y_{0.9}Cr_{0.1}NbO_4$ and $Y_{0.9}Ni_{0.05}NbO_{3.9}$ [Figure 3(f)], which should be regarded as metal-ion (Cr^{3+} and Ni^{2+}) doped yttrium niobates. That is true because of the distinct mismatch in valence states and ionic radii between Y^{3+} and Cr^{3+} or Ni^{2+} ions. The same situation also occurred in the $M_xNi_{1-x}Nb_2O_6$ (M = Sr, Ba) NPs. Excessive doping of metal ions was found to bring no changes in morphology and particle size, but much complicated alteration in the crystal phase for the synthesized niobate NPs, such as in the example of $YNiNb_3O_{10}$ NPs that were probably composed of multiphase and doped niobates (Figure S6). It remains unclear whether the multiphase niobates comprise separated NPs or exist together in one NP.

Because of its enhanced photocatalytic activity under visible light, the niobate solid solution $(AgNb)_{1-x}(SrTi)_xO_3$ attracts more attention. Unlike the niobates described above, it is difficult to incorporate all four metal elements – Ag, Nb, Sr, and Ti – into one NP directly by using only a one-step hydrothermal reaction, because silver ions would be preferentially reduced to metallic silver in aqueous solutions at high temperature. Therefore, we tried a two-step method to solve this problem, as portrayed schematically in Figure 4: First, amorphous compound N1 NPs containing Sr, Nb, Ti, and O were synthesized by a hydrothermal reaction; second, Sr ions in N1 NPs were partially exchanged by silver ions in aqueous solution to form amorphous compound N2 NPs (see the Experimental Section for details). Figure 5(a) portrays a SEM image of the amorphous compound N1 NPs for targeted production of niobate

$(AgNb)_{0.75}(SrTi)_{0.25}O_3$. The EDS spectrum of one single NP [Figure 5(b)] confirms that it contains the elements Sr, Nb, and Ti. After ion exchange, the SEM image of the N2 NPs [Figure 5(c)] shows that the morphology and particle size remain the same. Furthermore, the EDS spectrum of one single NP [Figure 5(d)] proves that the silver atoms entered it. The decrease in the intensity of the Sr peak relative to that of the Nb peak (0.5–0.38) means that some Sr^{2+} ions were consumed by exchange with Ag^+ ions in solution.

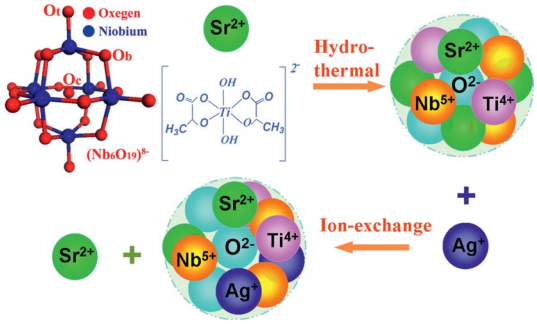

Figure 4. Schematic diagram: In the first step, amorphous N1 NPs containing Sr, Nb, Ti, and O were synthesized by a hydrothermal reaction. In the second step, Sr ions in N1 NPs were partially exchanged by silver ions in aqueous solution at 60 °C to form amorphous N2 NPs.

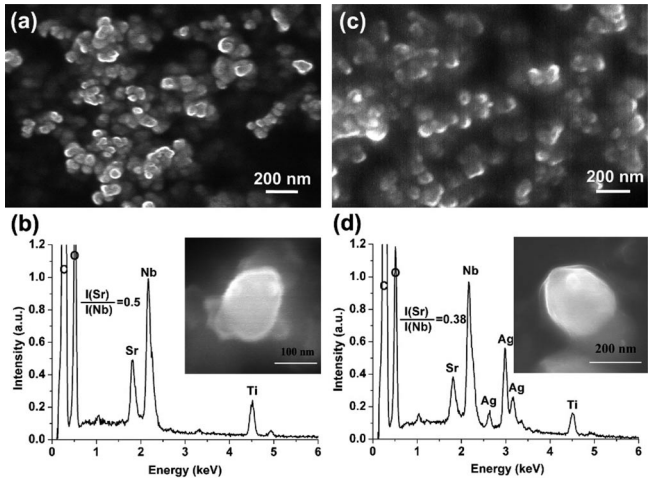

Figure 5. Silver/niobium-based amorphous compound NPs (before annealing) for synthesis of $(AgNb)_{0.75}(SrTi)_{0.25}O_3$ NPs: (a) SEM image and (b) EDS spectrum of one single NP (the inset is the SEM image) of amorphous N1 NPs; (c) SEM image and (d) EDS spectrum of one single NP (the inset is the SEM image) of the amorphous niobate N2 NPs attained by ion exchange between Sr^{2+} ions in N1 NPs and Ag^+ ions in aqueous solution.

For crystallization of $(AgNb)_{1-x}(SrTi)_xO_3$ NPs, the amorphous compound N2 NPs were calcined carefully. Figure 6(a) portrays a SEM image of $(AgNb)_{0.75}(SrTi)_{0.25}O_3$ NPs that were annealed at 650 °C for 24 h. It is apparent that changes in morphology and particle size of these NPs were rare after annealing, as were changes in composition based on the EDS spectrum of a single NP [Figure 6(b)]. However, at this time, the $(AgNb)_{0.75}(SrTi)_{0.25}O_3$ NPs were extremely sensitive to light and easily damaged under daylight irradiation. After additional calcination at 1000 °C for 24 h, they became more stable even under stronger light irradiation. The XRD patterns in Figure 6(c) show that the background curve became smoother, indicating that the crystallinity of the $(AgNb)_{0.75}(SrTi)_{0.25}O_3$ NPs had improved. The SEM image [Figure 6(d)] shows that the size of the $(AgNb)_{0.75}(SrTi)_{0.25}O_3$ NPs changed somewhat. However, if the amorphous compound N2 NPs were treated by one-step calcination at 1000 °C, the particle size would increase uncontrollably to nearly 1 μm [Figure 6(e)].

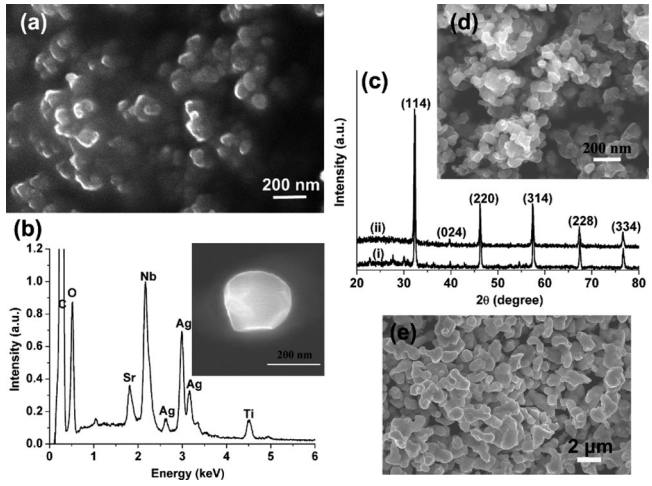

Figure 6. Nanocrystalline niobate $(AgNb)_{0.75}(SrTi)_{0.25}O_3$ obtained by calcination at 650 °C for 24 h: (a) SEM image, (b) EDS spectrum of one single NP (the inset shows a SEM image),(c) XRD pattern (i); XRD pattern with additional calcination at 1000 °C for 24 h (ii) (d) SEM image, and (e) SEM image of $(AgNb)_{0.75}(SrTi)_{0.25}O_3$ obtained by using one-step calcination at 1000 °C.

The $(AgNb)_{1-x}(SrTi)_xO_3$ solid solutions, when x is less than 0.9, retains an orthorhombic crystal structure with almost consistent lattice parameters,[4,5] as do the as-prepared $(AgNb)_{1-x}(SrTi)_xO_3$ NPs [Figure 7(a)]. Both bulk materials and $(AgNb)_{1-x}(SrTi)_xO_3$ NPs have similar UV/Vis absorption edges, which shift gradually from approximately 450 nm ($AgNbO_3$) to a shorter wavelength range with increasing Sr and Ti content. Within $x \leq 0.5$, the absorption edges are located at wavelengths longer than 420 nm [Figure 7(b)].

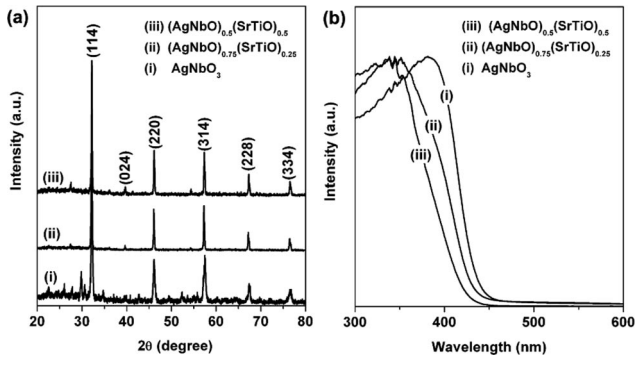

Figure 7. (a) XRD patterns and (b) UV/Vis absorption spectra of $AgNbO_3$, $(AgNb)_{0.75}(SrTi)_{0.25}O_3$, and $(AgNb)_{0.5}(SrTi)_{0.5}O_3$ NPs.

2.4 Photocatalytic Properties of As-Prepared Niobate NPs

2.4.1 Hydrogen Evolution over Yttrium-Based Niobate NPs

Photocatalytic hydrogen evolution from water over the yttrium-based niobate NPs under UV light irradiation has been studied. Here, platinum (Pt) was used as a cocatalyst loaded on niobate NPs, which is a generally accepted procedure in photocatalytic hydrogen production to enhance the catalytic efficiency greatly.[44] For example, Figure 8 shows that the photocatalytic activity of the Pt-loaded $YNbO_4$ NPs increased 40 times relative to that of the Pt-free ones. The $YNbO_4$ NPs produced about 10 times the amount of hydrogen over the $YNbO_4$ sample prepared by using a solid state reaction.[45] When the $YNbO_4$ NPs were taken as reference, the diversity in the photocatalytic performance of other quaternary yttrium-based niobate NPs [Figure 8(a)] was attributed to reconstruction of energy bands toward $YNbO_4$. The variations of band gaps are observable by tracing the UV/Vis absorption spectra [Figure 8(b)]. Results show that the absorption edges of $Y_{0.9}Cr_{0.1}NbO_4$ and $Y_{0.9}Ni_{0.05}NbO_{3.9}$ redshift, indicating they have narrower band gaps. No obvious difference was found between UV/Vis absorption spectra of $YNbO_4$ and $Y_{0.5}La_{0.5}NbO_4$. Figure 9 shows the band structures and projects the total density of states (DOS) of $YNbO_4$, $Y_{0.9}Cr_{0.1}NbO_4$, and $Y_{0.9}Ni_{0.05}NbO_{3.9}$, which were calculated by using the plane-wave-density function theory with the *CASTEP* program package. These simulations of energy structures (Figure 9) reveal that the energy band potentials of yttrium-based niobates are depressed because of the merging of a Cr 3d or Ni 3d electronic orbital into the conduction band, thereby narrowing the band gaps. The solid solution $Y_{0.5}La_{0.5}NbO_4$ NPs have more negative band potential than $YNbO_4$, as deduced from the band potential of $LaNbO_4$.[46] Figure 8(a) shows that the hydrogen production ability of the yttrium-based niobate NPs ranks as follows: $YNbO > Y_{0.5}La_{0.5}NbO_4 > Y_{0.9}Ni_{0.05}NbO_{3.9} > Y_{0.9}Cr_{0.1}NbO_4$. This ranking is in agreement with the common sense principle that more negative conduction potential might possess higher reductive activity, namely higher activity for hydrogen generation from water.

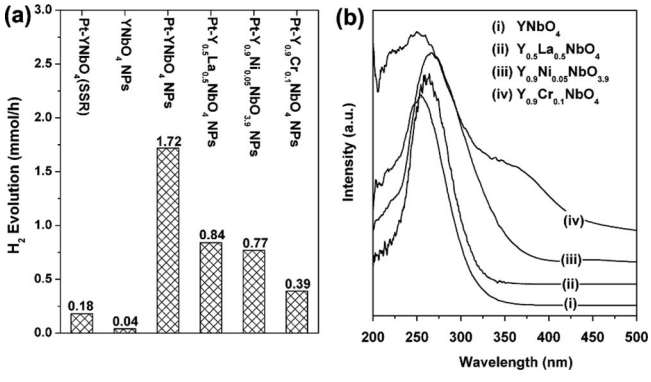

Figure 8. (a) Column diagram of hydrogen evolution per hour over yttrium-based niobate NPs (0.1 g) under UV light irradiation; (b) UV/Vis absorption spectra of the yttrium-based niobate NPs.

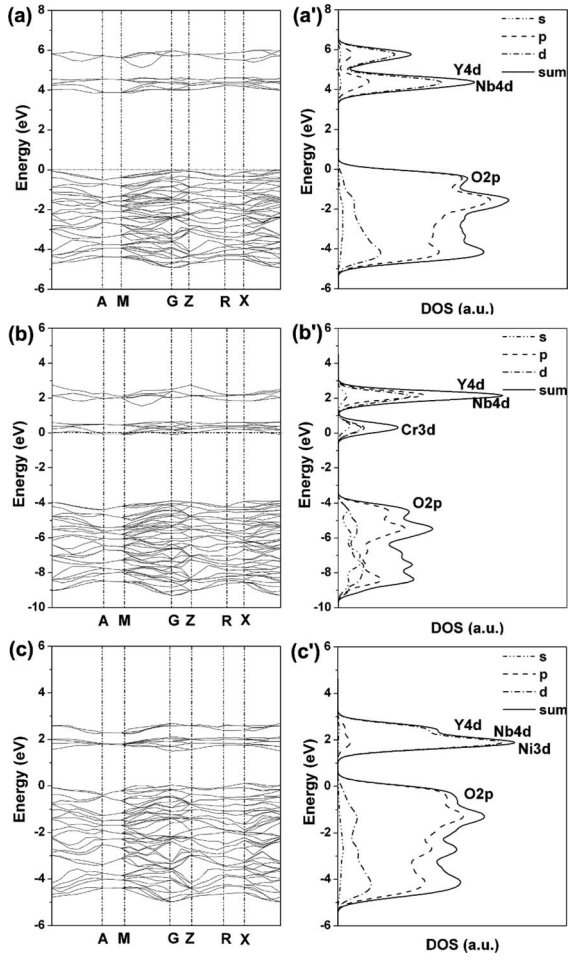

Figure 9. Calculated band structures and projected total density of states (DOS) for: (a,a′) $YNbO_4$, (b,b′) $Y_{0.9}Cr_{0.1}NbO_4$, (c,c′) $Y_{0.9}Ni_{0.05}NbO_{3.9}$.

2.4.2 Isopropyl Alcohol (IPA) Degradation over Solid Solution Niobate $(AgNb)_{1-x}(SrTi)_xO_3$ NPs

In our experiments, IPA decomposition under visible light ($\lambda > 420$ nm) was adopted to evaluate the photocatalytic activity of $(AgNb)_{1-x}(SrTi)_xO_3$ NPs. The photocatalytic decomposition process of IPA is fundamentally divided into two stages: $(CH_3)_2CHOH \rightarrow CH_3COCH_3 \rightarrow CO_2$. Over the three samples of $AgNbO_3$, $(AgNb)_{0.75}(SrTi)_{0.25}O_3$, and $(AgNb)_{0.5}(SrTi)_{0.5}O_3$ NPs, the respective evolutions of photocatalytic decomposition of IPA are presented in Figure 10(a) for acetone and Figure 10(b) for CO_2. The results show that these $(AgNb)_{1-x}(SrTi)_xO_3$ NPs have high activity for transformation of IPA to acetone. The best are the $(AgNb)_{0.75}(SrTi)_{0.25}O_3$ NPs, producing about 500 ppm acetone in the first hour over 0.2 g of photocatalyst, which was a better performance than that of the bulk materials. However, these $(AgNb)_{1-x}(SrTi)_xO_3$ NPs had low efficiency of converting acetone to CO_2, e.g. the best ones, $AgNbO_3$ NPs, gave off only 15 ppm of CO_2 per hour over 0.2 g of photocatalyst [Figure 10(b)]. Regarded comparatively, 0.4 g of $(AgNb)_{0.75}(SrTi)_{0.25}O_3$ prepared by solid re-

action can release more than one hundred ppm of CO_2 per hour.[4] The solution of this problem remains our ongoing task.

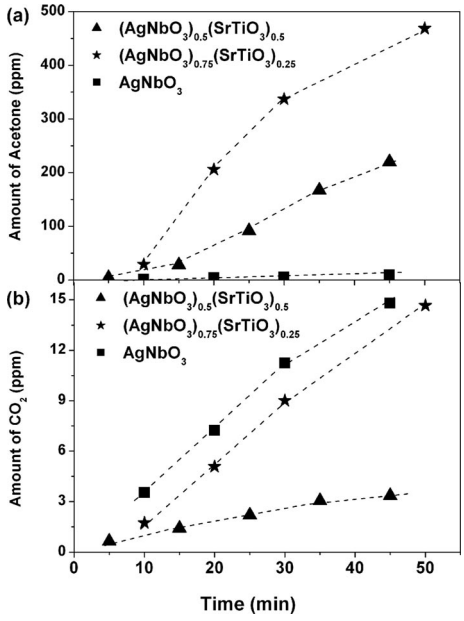

Figure 10. Evolution of photocatalytic decomposition of IPA for three samples: $AgNbO_3$, $(AgNb)_{0.75}(SrTi)_{0.25}O_3$, and $(AgNb)_{0.5}(SrTi)_{0.5}O_3$ NPs. Photocatalyst: 0.2 g; light source: 300 W Xe lamp with L42 and water filters; initial IPA concentration: approximately 400 ppm.

3. Conclusion

We present a general method for the synthesis of nanocrystalline niobates by using hexaniobate ions as a niobium source. The synthesis proceeded in two steps: soft-chemical synthesis and annealing crystallization. In the first step, microwave-assisted hydrothermal reaction produced amorphous compound NPs, of which the morphology, particle size, and amorphous atomic framework were defined by the polymerization of hexaniobate ions and for which the composition was controlled by the addition of reagents. In the second step, these amorphous compound NPs served as parent bodies, affording not only the nanoscale size but also the optimal compositions and elements for the final annealed nanocrystalline niobates. By this method, a series of nanocrystalline niobates, including $MNbO_4$ (M = In, Ga, Fe), MNb_2O_6 (M = Ba, Sr, Ni, Cd, Pb), $M_xFe_{1-x}NbO_4$ (M = In, Ga), $M_xNi_{1-x}Nb_2O_6$ (M = Ba, Sr), and $(AgNb)_{1-x}(SrTi)_xO_3$, was prepared. Our experimental results show that the compositions and elements of the nanocrystalline niobates are adjustable to produce strong influences on the crystal phase, energy band structure, and photocatalytic performance of the nanocrystalline niobates. The method described herein is expandable to design and synthesis of other types of nanocrystalline niobates as one might desire. Furthermore, it is expected that specially shaped or hierarchically assembled niobate nanomaterials will be achieved with the hexaniobate ions involved in this synthesis.

Experimental Section

Preparation of the Non-Alkali-Metal Hexaniobate Aqueous Solution: $NbCl_5$ (5 g) was dissolved in anhydrous ethanol (100 mL, 99.5%), into which a mixture (total volume: 50 mL) of ethanolamine (10 mL) and distilled water was added to generate amorphous $Nb_2O_5{\cdot}xH_2O$ precipitates immediately. After 20 min, the $Nb_2O_5{\cdot}xH_2O$ precipitates were collected by centrifugation, washed with ethanol (95%), and dispersed in a mixture (500 mL) of ethanolamine (10 mL) and distilled water (the treatments described above were performed at room temperature). This slurry solution was heated at 60 °C with magnetic stirring for 24 h to ensure a thoroughly transparent and colorless aqueous solution of hexaniobate ions.

Synthesis of Niobate NPs: Citric acid (2 g) was added to an aqueous solution (50 mL) of hexaniobate ions (containing 1.85 mmol niobium), and this was followed by stoichiometric addition of metal nitrate(s) for the targeted niobate [e.g., 1.85 mmol $Y(NO_3)_3{\cdot}4H_2O$ was added for $YNbO_4$ or 1.76 mmol $Y(NO_3)_3{\cdot}4H_2O$ and 0.09 mmol $Cr(NO_3)_3{\cdot}9H_2O$ were added for $Y_{0.9}Cr_{0.1}NbO_4$]. This clear precursor solution was transferred into an autoclave and treated in a microwave reactor (Microwave Laboratory System; Milestone General K.K., Japan) by following a program of heating to 220 °C in 10 min and maintaining the temperature at 220 °C for 50 min. After the solution cooled, the solid products (amorphous compound NPs) were separated by centrifugation and washed with ethanol and distilled water three times, and then dried at 70 °C. The dried and well-ground amorphous compound NPs were placed directly in an electric oven at a high temperature of 800 °C for 20 min for crystallization.

Synthesis of $(AgNb)_{1-x}(SrTi)_xO_3$ NPs: Amorphous compound N1 NPs containing Nb, Sr, and Ti were synthesized by microwave-assisted hydrothermal reaction as described above. Typically, citric acid (2 g) was added to an aqueous solution (50 mL) of hexaniobate ions (containing 1.85 mmol of niobium), and the composition of amorphous compound N1 NPs was controlled by adjusting the addition of the reagents Nb, Sr, and Ti in the molar ratios 6:3:0 for $AgNbO_3$, 6:5:2 for $(AgNb)_{0.75}(SrTi)_{0.25}O_3$, and 6:9:6 for $(AgNb)_{0.5}(SrTi)_{0.5}O_3$ in the solutions, respectively. Ion exchange between Sr^{2+} ions in N1 NPs and Ag^+ ions in an aqueous solution (in a Ag/Nb mol ratio of 1:1) was performed at 60 °C for 48 h to form amorphous compound N2 NPs. The amorphous compound N2 NPs were separated by centrifugation, washed with ethanol and distilled water three times, and dried at 70 °C for 12 h. Then they were well ground. Then the N2 NPs were calcined at 650 °C for 24 h and well ground after cooling. Finally, niobate NPs were calcined again at 1000 °C for 24 h.

Characterization: The prepared samples were characterized by using X-ray diffraction (Cu-K_α radiation, JDX-3500; JEOL, Japan), UV/Vis diffuse reflectance spectroscopy (UV-2500PC; Shimadzu Corp., Japan), SEM (JSM-6701F; JEOL, Japan), EDS (JED-2300 energy dispersive X-ray analyzer; JEOL, Japan), TEM (2000FX; JEOL, Japan), Raman spectroscopy (NRS-1000 laser Raman spectrophotometer; Jasco Inc., Japan), and IR spectroscopy (IR Prestige-21 Fourier transform infrared spectrophotometer; Shimadzu Corp., Japan).

Evaluation of Photocatalytic Activity: The photocatalytic H_2 evolution occurring over the samples of yttrium-based niobate NPs was investigated in a closed gas circulation system. Each photocatalyst (0.1 g) was dispersed and suspended by using a magnetic stirrer in a mixed solution of methanol (50 mL) and distilled water (320 mL), in which H_2PtCl_6 (1 wt.-%, Pt in photocatalyst) was added as a co-

catalyst. An inner 400 W high-pressure Hg lamp was used for light irradiation. The evolved H_2 was measured by using agas chromatograph (GC-8A; Shimadzu Corp.) with a thermal conductivity detector (TCD) . The test of photocatalytic decomposition of IPA over the silver-based niobate NPs was performed in a cylindrical air-filled static Pyrex glass vessel (total volume 500 mL). The photocatalyst (0.2 g) was spread over an area of about 8 cm^2 on the bottom of a circular glass dish in the vessel. After sealing the vessel, the air in it was replaced thoroughly with artificial pure air to prevent interference from CO_2 in air. Gaseous IPA (ca. 400 ppm) was injected into the vessel. Before absorption balancing of IPA on the photocatalyst, the vessel was kept in the dark. A 300 W Xenon arc lamp, used as the light source, was equipped with L42 and water filters to provide visible light irradiation. For testing the transformation of IPA to acetone and CO_2, a gaseous sample (5 μL) was extracted each time from the vessel and injected into a gas chromatograph (GC-14B; Shimadzu Corp.) for analysis.

Supporting Information (see footnote on the first page of this article): XRD patterns, SEM images, EDS spectra, TG-DTA curves.

Acknowledgments

This work was in part supported by the World Premier International Research Center Initiative on Materials Nanoarchitectonics, the Ministry of Education, Culture, Sport, Science and Technology (MEXT), and the Strategic International Cooperative Program, Japan Science and Technology Agency (JST), Japan.

[1] A. Fujishima, K. Honda, *Nature* **1972**, *238*, 37–38.
[2] Z. G. Zou, J. H. Ye, K. Sayama, H. Arakawa, *Nature* **2001**, *414*, 625–627.
[3] H. Kato, K. Asakura, A. Kudo, *J. Am. Chem. Soc.* **2003**, *125*, 3082–3089.
[4] D. F. Wang, T. Kako, J. H. Ye, *J. Phys. Chem. C* **2009**, *113*, 3785–3792.
[5] D. F. Wang, T. Kako, J. H. Ye, *J. Am. Chem. Soc.* **2008**, *130*, 2724–2725.
[6] X. K. Li, N. Kikugawa, J. H. Ye, *Adv. Mater.* **2008**, *20*, 3816–3819.
[7] F. E. Osterloh, *Chem. Mater.* **2008**, *20*, 35–54.
[8] R. M. Navarro, M. C. Sánchez-Sánchez, M. C. Alvarez-Galvan, F. del Valle, J. L. G. Fierro, *Energy Environ. Sci.* **2009**, *2*, 35–54.
[9] Z. S. Li, T. Yu, Z. G. Zou, J. H. Ye, *Appl. Phys. Lett.* **2006**, 88–90.
[10] Q. P. Ding, Y. P. Yuan, X. Xiong, R. P. Li, H. B. Huang, Z. S. Li, T. Yu, Z. G. Zou, S. G. Yang, *J. Phys. Chem. C* **2008**, *112*, 18846–18848.
[11] G. K. Zhang, F. S. He, X. Zou, J. Gong, H. B. Tu, H. Zhang, Q. Zhang, Y. Liu, *J. Alloys Compd.* **2007**, *427*, 82–86.
[12] R. Z. Ma, Y. Kobayashi, W. J. Youngblood, T. E. Mallouk, *J. Mater. Chem.* **2008**, *18*, 5982–5985.
[13] G. K. Zhang, F. S. He, X. Zou, J. Gong, H. Zhang, *J. Phys. Chem. Solids* **2008**, *69*, 1471–1474.
[14] Q. M. Wei, T. Nakato, *J. Porous Mater.* **2009**, *16*, 151–156.
[15] D. Chen, J. H. Ye, *Chem. Mater.* **2009**, *21*, 2327–2333.
[16] O. C. Compton, F. E. Osterloh, *J. Phys. Chem. C* **2009**, *113*, 479–485.
[17] K. Maeda, M. Eguchi, S. H. A. Lee, W. J. Youngblood, H. Hata, T. E. Mallouk, *J. Phys. Chem. C* **2009**, *113*, 7962–7969.
[18] O. C. Compton, E. C. Carroll, J. Y. Kim, D. S. Larsen, F. E. Osterloh, *J. Phys. Chem. C* **2007**, *111*, 14589–14592.
[19] L. Z. Zhang, I. Djerdj, M. H. Cao, M. Antonietti, M. Niederberger, *Adv. Mater.* **2007**, *19*, 2083–2086.
[20] G. Z. Wang, Y. D. Yu, T. Grande, M. A. Einarsrud, *J. Nanosci. Nanotechnol.* **2009**, *9*, 1465–1469.
[21] K. Bhattacharyya, A. K. Tyagi, *J. Alloys Compd.* **2009**, *470*, 580–583.
[22] B. D. Wood, V. Mocanu, B. D. Gates, *Adv. Mater.* **2008**, *20*, 4552–4556.
[23] A. J. Paula, R. Parra, M. A. Zaghete, J. A. Varela, *Mater. Lett.* **2008**, *62*, 2581–2584.
[24] Y. M. Hu, H. S. Gu, Z. L. Hu, W. N. Di, Y. Yuan, J. You, W. Q. Cao, Y. Wang, H. L. W. Chan, *Cryst. Growth Des.* **2008**, *8*, 832–837.
[25] O. C. Compton, C. H. Mullet, S. Chiang, F. E. Osterloh, *J. Phys. Chem. C* **2008**, *112*, 6202–6208.
[26] H. Y. Zhu, Z. F. Zheng, X. P. Gao, Y. N. Huang, Z. M. Yan, J. Zou, H. M. Yin, Q. D. Zou, S. H. Kable, J. C. Zhao, Y. F. Xi, W. N. Martens, R. L. Frost, *J. Am. Chem. Soc.* **2006**, *128*, 2373–2384.
[27] S. Wohlrab, M. Weiss, H. C. Du, S. Kaskel, *Chem. Mater.* **2006**, *18*, 4227–4230.
[28] I. Pribosic, D. Makovec, M. Drofenik, *Chem. Mater.* **2005**, *17*, 2953–2958.
[29] C. Sun, X. R. Xing, J. Chen, J. X. Deng, L. Li, R. B. Yu, L. J. Qiao, G. R. Liu, *Eur. J. Inorg. Chem.* **2007**, 1884–1888.
[30] M. Nyman, T. M. Anderson, P. P. Provencio, *Cryst. Growth Des.* **2009**, *9*, 1036–1040.
[31] C. A. Ohlin, E. M. Villa, W. H. Casey, *Inorg. Chim. Acta* **2009**, *362*, 1391–1392.
[32] E. M. Villa, C. A. Ohlin, E. Balogh, T. M. Anderson, M. D. Nyman, W. H. Casey, *Am. J. Sci.* **2008**, *308*, 942–953.
[33] C. Y. Xu, L. Zhen, R. Yang, Z. L. Wang, *J. Am. Chem. Soc.* **2007**, *129*, 15444–15445.
[34] N. Wei, D. M. Zhang, X. Y. Han, F. X. Yang, Z. C. Zhong, K. Y. Zheng, *J. Am. Ceram. Soc.* **2007**, *90*, 1434–1437.
[35] G. Q. Li, T. Kako, D. F. Wang, Z. G. Zou, J. Ye, *J. Solid State Chem.* **2007**, *180*, 2845–2850.
[36] M. Maekawa, Y. Ozawa, A. Yagasaki, *Inorg. Chem.* **2006**, *45*, 9608–9609.
[37] J. Y. Niu, P. T. Ma, H. Y. Niu, J. Li, J. W. Zhao, Y. Song, J. P. Wang, *Chem. Eur. J.* **2007**, *13*, 8739–8748.
[38] R. P. Bontchev, M. Nyman, *Angew. Chem. Int. Ed.* **2006**, *45*, 6670–6672.
[39] A. Goiffon, E. Philippot, M. Maurin, *Rev. Chim. Miner.* **1980**, *17*, 466–476.
[40] F. J. Farrell, V. A. Maroni, T. G. Spiro, *Inorg. Chem.* **1969**, *8*, 2638–2642.
[41] M. Nyman, M. A. Rodriguez, T. M. Alam, T. M. Anderson, A. Ambrosini, *Chem. Mater.* **2009**, *21*, 2201–2208.
[42] M. Nyman, M. A. Rodriguez, L. E. Shea-Rohwer, J. E. Martin, P. P. Provencio, *J. Am. Chem. Soc.* **2009**, *131*, 11652–11653.
[43] G. K. Zhang, Y. J. Hu, X. M. Ding, J. Zhou, J. W. Xie, *J. Solid State Chem.* **2008**, *181*, 2133–2138.
[44] M. Yoshida, A. Yamakata, K. Takanabe, J. Kubota, M. Osawa, K. Domen, *J. Am. Chem. Soc.* **2009**, *131*,13218–13219.
[45] C. Pithan, Y. Shiratori, J. Dornseiffer, F. H. Haegel, A. Magrez, R. Waser, *J. Cryst. Growth* **2005**, *280*, 191–200.
[46] D. E. Scaife, *Sol. Energy* **1980**, *25*, 41–54.

Received: November 21, 2009
Published Online: February 22, 2010

